HHS Public Access

Author manuscript

Eur J Radiol. Author manuscript; available in PMC 2016 May 11.

Published in final edited form as:

Eur J Radiol. 2016 April ; 85(4): 700–706. doi:10.1016/j.ejrad.2016.02.004.

Diffusion tensor imaging suggests extrapontine extension of pediatric diffuse intrinsic pontine gliomas

Matthias W. Wagner[a,b], **W. Robert Bell**[c], **Jason Kern**[c], **Thangamadhan Bosemani**[a], **Joyce Mhlanga**[a], **Kathryn A. Carson**[e,f], **Kenneth J. Cohen**[d], **Eric H. Raabe**[c,d], **Fausto Rodriguez**[c], **Thierry A.G.M. Huisman**[a], and **Andrea Poretti**[a,*]

[a]Section of Pediatric Neuroradiology, Division of Pediatric Radiology, Russell H. Morgan Department of Radiology and Radiological Science, The Johns Hopkins University School of Medicine, Baltimore, MD, USA [b]Department of Diagnostic and Interventional Radiology, University Hospital Zurich, Zurich, Switzerland [c]Department of Pathology, The Johns Hopkins University School of Medicine, Baltimore, MD, USA [d]Division of Pediatric Oncology, The Sidney Kimmel Comprehensive Cancer Center at Johns Hopkins, The Johns Hopkins University School of Medicine, Baltimore, MD, USA [e]Department of Epidemiology, The Johns Hopkins Bloomberg School of Public Health, Baltimore, MD, USA [f]Division of General Internal Medicine, Department of Medicine, The Johns Hopkins School of Medicine, Baltimore, Maryland, USA

Abstract

Purpose—To apply DTI to detect early extrapontine extension of pediatric diffuse intrinsic pontine glioma along the corticospinal tracts.

Methods—In children with diffuse intrinsic pontine glioma, low-grade brainstem glioma, and age-matched controls, DTI metrics were measured in the posterior limb of the internal capsule and posterior centrum semiovale. Histological examination was available in one patient.

Results—6 diffuse intrinsic pontine glioma, 8 low-grade brainstem glioma, and two groups of 25 controls were included. In diffuse intrinsic pontine glioma compared to controls, fractional anisotropy was lower in the bilateral posterior limb of the internal capsule, axial diffusivity was lower in the bilateral posterior centrum semiovale and posterior limb of the internal capsule, while radial diffusivity was higher in the bilateral posterior limb of the internal capsule. No significant differences were found between low-grade brainstem glioma and controls. In diffuse intrinsic pontine glioma compared to low-grade brainstem glioma, axial diffusivity was lower in the bilateral posterior limb of the internal capsule. Histological examination in one child showed tumor cells in the posterior limb of the internal capsule.

Conclusion—Reduction in fractional anisotropy and axial diffusivity and increase in radial diffusivity in diffuse intrinsic pontine glioma may reflect tumor extension along the corticospinal

[*]Corresponding author at: Section of Pediatric Neuroradiology, Division of Pediatric Radiology, Russell H. Morgan Department of Radiology and Radiological Science, Charlotte R. Bloomberg Children's Center, Sheikh Zayed Tower, Room 4174, 1800 Orleans Street, Baltimore, MD 21287-0842, USA. Fax: +1 410 502 3633. aporett1@jhmi.edu (A. Poretti).

Appendix A. Supplementary data

Supplementary data associated with this article can be found, in the online version, at http://dx.doi.org/10.1016/j.ejrad.2016.02.004.

tracts as shown by histology. DTI may detect early extrapontine tumor extension in diffuse intrinsic pontine glioma before it becomes apparent on conventional MRI sequences.

Keywords

Children; Diffusion tensor imaging; Diffuse intrinsic pontine glioma; Neuroimaging; Corticospinal tract; Extrapontine extension

1. Introduction

Diffuse intrinsic pontine glioma (DIPG) is the most common pediatric brain stem tumor and accounts for about 10% of all brain tumors in children [1]. Affected children present typically with a short duration of symptoms (less than 6 months) including cranial nerve palsy (especially VI and VII), long tract signs (hyperreflexia and Babinski sign), and cerebellar signs (ataxia, dysmetria, or dysarthria) [2]. Neuroimaging plays a key role in the diagnostic process of DIPG and these tumors are typically diagnosed based on imaging characteristics alone. The classic MRI findings include pontine enlargement with tumor centered in and involving more than 50–70% of the cross sectional area of the pons, hypointense signal on T1-, and hyperintense signal on T2-weighted images [3]. In addition, anterior exophytic extension with “embracement” of the basilar artery, extension into the midbrain and middle cerebellar peduncles, and contrast enhancement are common in DIPG. The prognosis is generally poor and without radiotherapy, the median survival is approximately four months [4,5]. On conventional MRI, extrapontine tumor extension is present in 13% of patients at median post-diagnostic time of 7.2 months [6]. Early detection of extrapontine tumor extension in DIPG may be of biological relevance and lead to changes in management and treatment for these tumors in children (e.g. less focal radiotherapy with radiosensitive chemotherapy).

Low-grade brain stem glioma (LGBG) are low-grade astrocytomas and account for about 15–20% of brain stem tumors [7]. They have a long duration of symptoms before diagnosis, growth patterns of low-grade glial tumors, and follow an indolent course [7,8]. LGBG are focal or grow dorsally exophytic, but in contrast to DIPG do not infiltrate the brainstem white matter tracts [9].

DTI is an advanced MRI technique that allows in vivo evaluation of the microstructure and integrity of white matter tracts [10,11]. DTI has been shown to be highly sensitive in detecting white matter abnormalities that are not visible on conventional, contrast-enhanced MRI sequences and is therefore a suitable technique to study white matter changes secondary to extrapontine tumor extension along the corticospinal tracts (CST) in DIPG, even before abnormalities are noted on conventional MRI [12].

The aim of this study was to compare the microstructural integrity of the supratentorial white matter tracts using DTI in children with (1) DIPG, (2) LGBG, and (3) healthy controls. We hypothesized changes in DTI parameters in children with DIPG representing early extrapontine tumor extension along the CST that are not (yet) visible on conventional MRI sequences in the majority of patients.

2. Materials and methods

This retrospective study was approved by the institutional review board (Johns Hopkins School of Medicine eIRB protocol NA 00092056).

2.1. Study population

The inclusion criteria for this study were: (1) diagnosis of DIPG based on neuroimaging (pontine enlargement with the tumor centered in and involving more than 50–70% of the cross sectional area of the pons, hypointense signal on T1-, and hyperintense signal on T2-weighted images) [3] and LGBG based on histology (defined as non-DIPG low-grade brain stem gliomas), (2) absence of T1-weighted hypointense and T2-weighted/fluid attenuation inversion recovery (FLAIR) hyperintense extrapontine tumor extension along the CST at diagnosis, (3) availability of pre-treatment DTI data without artifacts enabling high quality post-processing, and (4) age at MRI 18 years and younger. Data from eligible patients were collected through an electronic search of our pediatric neuroradiology database covering the time period between September 1, 2010, and September 30, 2014. Demographic data of the patients were collected by a review of the clinical histories.

Controls were selected from our pediatric MRI database using the following criteria: (1) normal brain anatomy, (2) absence of neurological disorders, and (3) availability of DTI raw data.

2.1.1. Diffusion tensor imaging—All MRI studies were performed on a 1.5 T MRI scanner (Siemens, Erlangen, Germany) using our standard departmental protocol including isotropic 3D-T1-weighted, axial T2-weighted and FLAIR images, axial, coronal, and sagittal T1-weighted images after intravenous injection of a Gadolinium-based contrast agent, and a single shot spin echo, echo planar axial DTI sequence with diffusion gradients along 20 non-collinear directions. An effective high **b**-value of 1000 s/mm^2 was used for each of the 20 diffusion-encoding directions. We performed an additional measurement without diffusion weighting (**b** = 0 s/mm^2). For the acquisition of the DTI data, the following parameters were used: TR = 7100 ms, TE = 84 ms, slice thickness = 2.5 mm, FOV = 240 × 240 mm, and MS = 192 × 192. Parallel imaging iPAT = 2 with Generalized Auto-Calibrating Partial Parallel Acquisition reconstruction was used. The acquisition was repeated twice to enhance SNR ratio.

2.1.2. DTI analysis—DTI data of the patients were transferred to an off-line work-station for further post-processing. DtiStudio, DiffeoMap and RoiEditor software (freely available at www.MriStudio.org) were used. The raw diffusion images were first co-registered to one of the least images and corrected for eddy current artifacts and subject motion using a 12-mode affine transformation. The following maps were generated: fractional anisotropy (FA), vector, color-coded FA, mean (MD), axial (AD), and radial (RD) diffusivity. After rigid transformation to an age-appropriate template for adjustment of position and rotation of images, ROIs were drawn manually by the first author (MWW) and centered within the bilateral posterior limb of the internal capsule (PLIC) and posterior centrum semiovale (PCSO), where the CSTs are known to course (Fig. 1). Proper placement of the ROIs was confirmed by the senior author (AP), a pediatric neurologist with 7 years of experience in

DTI research. For the identification of each structure, axial color-coded FA maps were used and compared to the MRI atlas by Oishi et al. [13]. For each analyzed structure, three different ROIs on contiguous MR slices were placed and the average FA, MD, AD, and RD values were calculated. Each ROI was drawn as large as possible on axial color-coded images.

2.1.3. Histology—Histologic sections were obtained post-mortem from a single case of DIPG in a 6 year-old female. Tissue sections from the cerebral cortex, basal ganglia, basal forebrain, thalamus, bilateral PLIC, bilateral PCSO, hippocampus, entorhinal cortex, midbrain, pons, medulla, spinal cord, and cerebellum were taken, fixed with formalin, and stained with H&E. For all patients with LGBG, the diagnosis was made histologically by neuropathologists on biopsy specimens obtained at the time of diagnosis.

2.1.4. Statistical analysis—Two-sample *t*-tests were used to test for differences in age between (1) children with DIPG and controls, (2) children with LGBG and controls, and (3) children with DIPG and LGBG. DTI scalars were summarized using means and standard deviations. Wilcoxon rank sum tests were used to test for differences in DTI scalars between patients and controls because of the small sample sizes. However, general linear models regression was used to compare DTI scalars of children with DIPG and LGBG to allow for age adjustment. These data were summarized using least squares means and 95% CIs and compared using F-tests. Analyses were performed using SAS version 9.3 (SAS Institute, Inc., Cary, NC, USA) and MATLAB (The MathWorks, Inc., Natick, MA, USA). All tests were two-sided and observed differences were considered statistically significant if $p < 0.05$. No adjustment was made for multiple comparisons.

3. Results

3.1. Participants

The study included 6 children with DIPG (mean age at MRI, 5.74 ± 1.28 years, 3 females), 8 children with LGBG (mean age at MRI, 8.82 ± 3.23 years, 5 females), and 50 controls (mean age, 7.28 ± 2.02 years, 23 females). The 50 controls were divided in 2 groups of each 25 children (mean age 5.74 ± 1.14 years and 8.82 ± 1.14 years, respectively) that were group age-matched to the DIPG and LGBG patients, respectively. No differences were found in age between DIPG patients and their controls and LGBG and their controls, respectively ($p > 0.99$). The group-matching of controls was performed in order to compare the DTI parameters of children with different age.

At first presentation, children with DIPG had truncal ataxia (6/6), bilateral abducens nerve palsy (3/6), spasticity (unilateral 2/6, bilateral 1/6), and dysarthria (1/6). All patients were treated with radiation therapy. In addition, 5 out of 6 children had different chemotherapy regimens. Children with LGBG presented with hemiparesis (6/8), ataxia (2/8), torticollis (1/8), headaches (1/8), and hearing loss (1/8). All patients were treated by neurosurgery (biopsy in 6 children and subtotal resection in 2 patients, respectively). In addition, 7 children received different chemotherapy regimens and one child had a focal radiotherapy.

3.2. Imaging analysis

The DTI scalars for children with DIPG and age-matched controls are summarized and compared in Fig. 2 and Table 1. In children with DIPG we found a decrease in FA in the left and right PLIC compared to age-matched controls ($p = 0.001$ and $p < 0.001$, respectively), while no difference was observed in FA in the PCSO. MD was lower in DIPG patients compared to age-matched controls in the right PCSO ($p = 0.02$) and left PLIC ($p = 0.048$). In comparison to age-matched participants, AD was lower in DIPG patients in both left and right PCSO ($p = 0.02$ and $p = 0.01$, respectively) and left and right PLIC ($p = 0.001$ and $p < 0.001$, respectively), while RD was higher in the left and right PLIC (both $p = 0.02$).

The DTI scalars for children with LGBG and age-matched controls are summarized and compared in Supplemental Fig. 1 and Supplemental Table 1. In all regions, no significant differences were observed in DTI metrics between LGBG patients and comparison participants.

Age-adjusted least squares means and 95% CIs of DTI scalars for children with DIPG and LGBG are shown in Fig. 3 and Table 2. AD values were significantly lower in the left and right PLIC for children with DIPG compared to LGBG patients ($p = 0.049$ and $p = 0.03$, respectively), while in all regions, no differences were observed in FA, MD, and RD.

3.3. Histology

Post-mortem gross brain examination of one DIPG case revealed an ill-defined mass extending from upper medulla to thalamus, with distortion of the normal brain architecture. Sections from the main tumor bulk in the pons (Fig. 4A and B) showed hypercellularity with diffuse infiltration of hyperchromatic, atypical astrocytes. Mitotic activity was elevated (Fig. 4B), and areas of pseudopallisading necrosis were present, meeting criteria for glioblastoma, WHO Grade IV. Sections of the left PLIC showed infiltrating astrocytoma (Fig. 4C and D). Infiltrating tumor was not observed in the right PLIC. Tumor was also observed histologically in the medulla, midbrain, pons, and cerebellum.

Histological examination for 8 LGBG revealed three pilocytic astrocytoma, two low-grade astrocytoma, two low-grade glioma, and one low-grade fibrillary astrocytoma.

4. Discussion

In children with DIPG, DTI was shown to provide valuable information about tumor biology/extension that is not available from conventional MRI studies. In 9 children with DIPG, Chen et al. found lower FA and higher ADC values within the tumor compared to measurements within the normal brain stem or medulloblastoma [14]. This finding characterizes DIPG as a hypocellular tumor with extensive edema. High FA and low ADC values at diagnosis correlated with a worse clinical outcome. The correlation of DTI scalars at presentation and tumor behavior was confirmed by Lober et al. [15]. Helton et al. applied DTI to study brainstem white matter tracts involvement in 6 children with DIPG [16]. The authors found changes in DTI parameters (decrease in FA and increase in ADC) within the pontine CST, transverse pontine fibers, and medial lemnisci in patients compared to controls. Prabhu et al. evaluated serial changes in DTI scalars of the pontine white matter tracts in 3

children with DIPG [17]. The authors found transient increase in FA and decrease in ADC values during therapy and tumor response to treatment with subsequent drop in FA and marked increase in ADC at tumor progression. This longitudinal study suggests that initial changes in DTI scalars most likely reflect infiltration by tumor, while tumor progression results in complete loss of FA secondary to tract disruption [17].

In our study, we applied DTI to study the microstructural integrity of white matter tracts located outside the primary site of the pontine tumor. In children with DIPG, extrapontine tumor extension occurs in 13% of the patients after a median time of 7.2 months after diagnosis based on conventional contrast-enhanced MRI [6]. Previous studies in adults with glioblastomas showed that DTI has a higher sensitivity in detecting regions of tumor infiltration compared to contrast-enhanced MRI [18]. We hypothesized that early extrapontine tumor extension may be more common than detected by conventional MRI, including contrast enhanced MRI. To test this hypothesis, we compared DTI measurements in the PLIC and PCSO between children with DIPG and age-matched controls. We found decrease in FA and AD and increase in RD in the PLIC in patients compared to controls. These findings suggest disruption of the directional organization of fiber tracts and an increase in isotropic tissue structures at the level of the PLIC, which is consistent with invasion and injury of the white matter tract and increase in extracellular matrix by tumor cells. Glioma cells have been shown to produce their own extracellular matrix which plays a key role for tumor migration [19]. In addition, these changes in DTI parameters are similar to those reported by Helton et al. and Prabhu et al. suggesting tumor invasion of the pontine white matter tracts and tumor extension along the CST [16,17]. Glioma cells have a preferential extension and invasion pathway along white matter tracts: many of them cross the corpus callosum to form butterfly lesions, while other gliomas remain confined to the white matter, stopping abruptly at the gray-white-matter junction [20]. In a rat glioma model, iron-laden cells implanted close to the anterior commissure showed a clear tendency to migrate along white matter fiber tracts as detected by in vivo MRI [21]. Decrease in FA and AD and increase in RD in the PLIC, however, may also be explained by a secondary (Wallerian) degeneration of the CST due to tract disruption at the level of the primary site of the tumor within the pons [11].

To differentiate between tumor infiltration and secondary Wallerian degeneration, we analyzed DTI scalars within the same anatomical regions in children with biopsy-proven LGBG and age-matched controls. We did not find differences in DTI scalars between children with LGBG and age-matched controls. This result supports invasion and disruption of the white matter tract by tumor cells to explain differences in DTI scalars in the PLIC between children with DIPG and controls. LGBG are expected to locally injure the white matter tracts and cause secondary Wallerian degeneration, but not invade and remotely injure the white matter tracts by tumor cells due to the low-grade of malignancy. In addition, we compared the DTI scalars of children with DIPG and LGBG. We found lower AD values in the bilateral PLIC for children with DIPG compared to LGBG patients. AD represents diffusivity in the direction parallel to the white matter fibers [22,23]. Accordingly, decrease in AD is assumed to reflect axonal damage by tumor infiltration supporting our initial hypothesis. Finally, the postmortem histological findings in one child further indicate invasion by tumor cells at the level of the PLIC to explain changes in DTI scalars along the

CST in children with DIPG. However, Wallerian degeneration cannot be completely ruled out as a partial explanation of the changes in DTI scalars observed in our study.

We are aware of some limitations of our study, including the small number of patients, the retrospective nature of the study, the ROI based analysis, which is investigator dependent. An additional limitation is the difference in age distributions of children with DIPG and LGBG. However, we utilized regression analysis to adjust for age in our comparisons of DTI scalars in these patient groups.

5. Conclusion

Our study shows that quantitative DTI analysis may detect early extrapontine extension of tumor cells along and invasion of the CST at the level of the bilateral PLIC in children with DIPG while conventional MRI may fail to demonstrate tumor in the corresponding locations. This information may be helpful to monitor disease progression, guide treatment options and may help to better understand tumor biology. Larger studies including additional histology staining of the CST are warranted to confirm the quantitative DTI analysis.

Supplementary Material

Refer to Web version on PubMed Central for supplementary material.

Abbreviations

AD	axial diffusivity
PCSO	posterior centrum semiovale
CST	corticospinal tract
DIPG	diffuse intrinsic pontine glioma
FA	fractional anisotropy
LGBG	low-grade brain stem glioma
MD	mean diffusivity
PLIC	posterior limb of the internal capsule
RD	radial diffusivity.

References

1. Guillamo JS, Lisovoski F, Christov C, et al. Migration pathways of human glioblastoma cells xenografted into the immunosuppressed rat brain. J. Neurooncol. 2001; 52(3):205–215. [PubMed: 11519850]
2. Donaldson SS, Laningham F, Fisher PG. Advances toward an understanding of brainstem gliomas. J. Clin. Oncol. 2006; 24(8):1266–1272. [PubMed: 16525181]
3. Poretti A, Meoded A, Huisman TA. Neuroimaging of pediatric posterior fossa tumors including review of the literature. J. Magn. Reson. Imaging. 2012; 35(1):32–47. [PubMed: 21989968]
4. Lassman LP, Arjona VE. Pontine gliomas of childhood. Lancet. 1967; 1(7496):913–915. [PubMed: 4164397]

5. Conway AE, Reddick WE, Li Y, et al. Occult post-contrast signal enhancement in pediatric diffuse intrinsic pontine glioma is the MRI marker of angiogenesis? Neuroradiology. 2014; 56(5):405–412. [PubMed: 24626721]
6. Wagner S, Benesch M, Berthold F, et al. Secondary dissemination in children with high-grade malignant gliomas and diffuse intrinsic pontine gliomas. Br. J. Cancer. 2006; 95(8):991–997. [PubMed: 17047647]
7. Hargrave D, Bartels U, Bouffet E. Diffuse brainstem glioma in children: critical review of clinical trials. Lancet Oncol. 2006; 7(3):241–248. [PubMed: 16510333]
8. Ramos A, Hilario A, Lagares A, Salvador E, Perez-Nunez A, Sepulveda J. Brainstem gliomas. Semin. Ultrasound CT MR. 2013; 34(2):104–112. [PubMed: 23522775]
9. Jallo GI, Biser-Rohrbaugh A, Freed D. Brainstem gliomas. Childs Nerv. Syst. 2004; 20(3):143–153. [PubMed: 14669023]
10. Basser PJ. Inferring microstructural features and the physiological state of tissues from diffusion-weighted images. NMR Biomed. 1995; 8(7–8):333–344. [PubMed: 8739270]
11. Pierpaoli C, Barnett A, Pajevic S, et al. Water diffusion changes in Wallerian degeneration and their dependence on white matter architecture. Neuroimage. 2001; 13(6 Pt 1):1174–1185. [PubMed: 11352623]
12. Deng Z, Yan Y, Zhong D, et al. Quantitative analysis of glioma cell invasion by diffusion tensor imaging. J. Clin. Neurosci. 2010; 17(12):1530–1536. [PubMed: 20869249]
13. Oishi K, Faria AV, van Zijl PCM, Mori S. MRI Atlas of Human White Matter. Elsevier Science. 2010
14. Chen HJ, Panigrahy A, Dhall G, Finlay JL, Nelson MD Jr, Bluml S. Apparent diffusion and fractional anisotropy of diffuse intrinsic brain stem gliomas. AJNR Am. J. Neuroradiol. 2010; 31(10):1879–1885. [PubMed: 20595371]
15. Lober RM, Cho YJ, Tang Y, et al. Diffusion-weighted MRI derived apparent diffusion coefficient identifies prognostically distinct subgroups of pediatric diffuse intrinsic pontine glioma. J. Neurooncol. 2014; 117(1):175–182. [PubMed: 24522717]
16. Helton KJ, Phillips NS, Khan RB, et al. Diffusion tensor imaging of tract involvement in children with pontine tumors. AJNR Am. J. Neuroradiol. 2006; 27(4):786–793. [PubMed: 16611765]
17. Prabhu SP, Ng S, Vajapeyam S, et al. DTI assessment of the brainstem white matter tracts in pediatric BSG before and after therapy: a report from the Pediatric Brain Tumor Consortium. Childs Nerv. Syst. 2011; 27(1):11–18. [PubMed: 21052693]
18. Gerstner ER, Chen PJ, Wen PY, Jain RK, Batchelor TT, Sorensen G. Infiltrative patterns of glioblastoma spread detected via diffusion MRI after treatment with cediranib. Neuro Oncol. 2010; 12(5):466–472. [PubMed: 20406897]
19. Bouterfa H, Darlapp AR, Klein E, Pietsch T, Roosen K, Tonn JC. Expression of different extracellular matrix components in human brain tumor and melanoma cells in respect to variant culture conditions. J. Neurooncol. 1999; 44(1):23–33. [PubMed: 10582665]
20. Louis DN. Molecular pathology of malignant gliomas. Annu. Rev. Pathol. 2006; 1:97–117. [PubMed: 18039109]
21. Zhang F, Xie J, Liu G, He Y, Lu G, Chen X. In vivo MRI tracking of cell invasion and migration in a rat glioma model. Mol. Imaging Biol. 2011; 13(4):695–701. [PubMed: 20717735]
22. Alexander AL, Lee JE, Lazar M, et al. Diffusion tensor imaging of the corpus callosum in Autism. Neuroimage. 2007; 34(1):61–73. [PubMed: 17023185]
23. Alexander AL, Lee JE, Lazar M, Field AS. Diffusion tensor imaging of the brain. Neurotherapeutics. 2007; 4(3):316–329. [PubMed: 17599699]

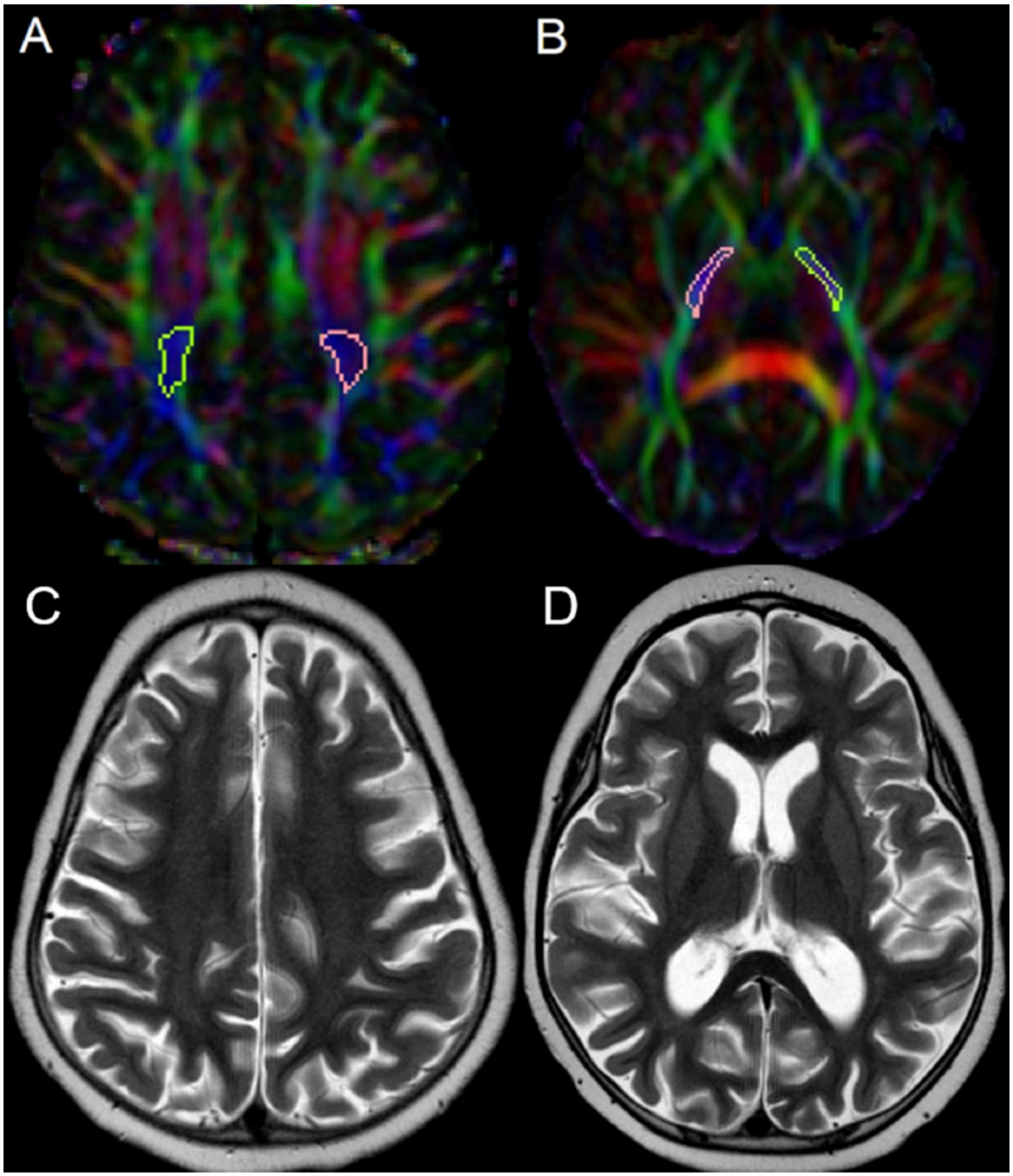

Fig. 1.

Axial color-coded fractional anisotropy (FA) maps (A, B) show the position of the regions of interest covering the bilateral posterior limb of the posterior centrum semiovale (PCSO) and internal capsule (PLIC). Axial T2-weighted images of the same patient at the level of the PCSO (C) and PLIC (D).

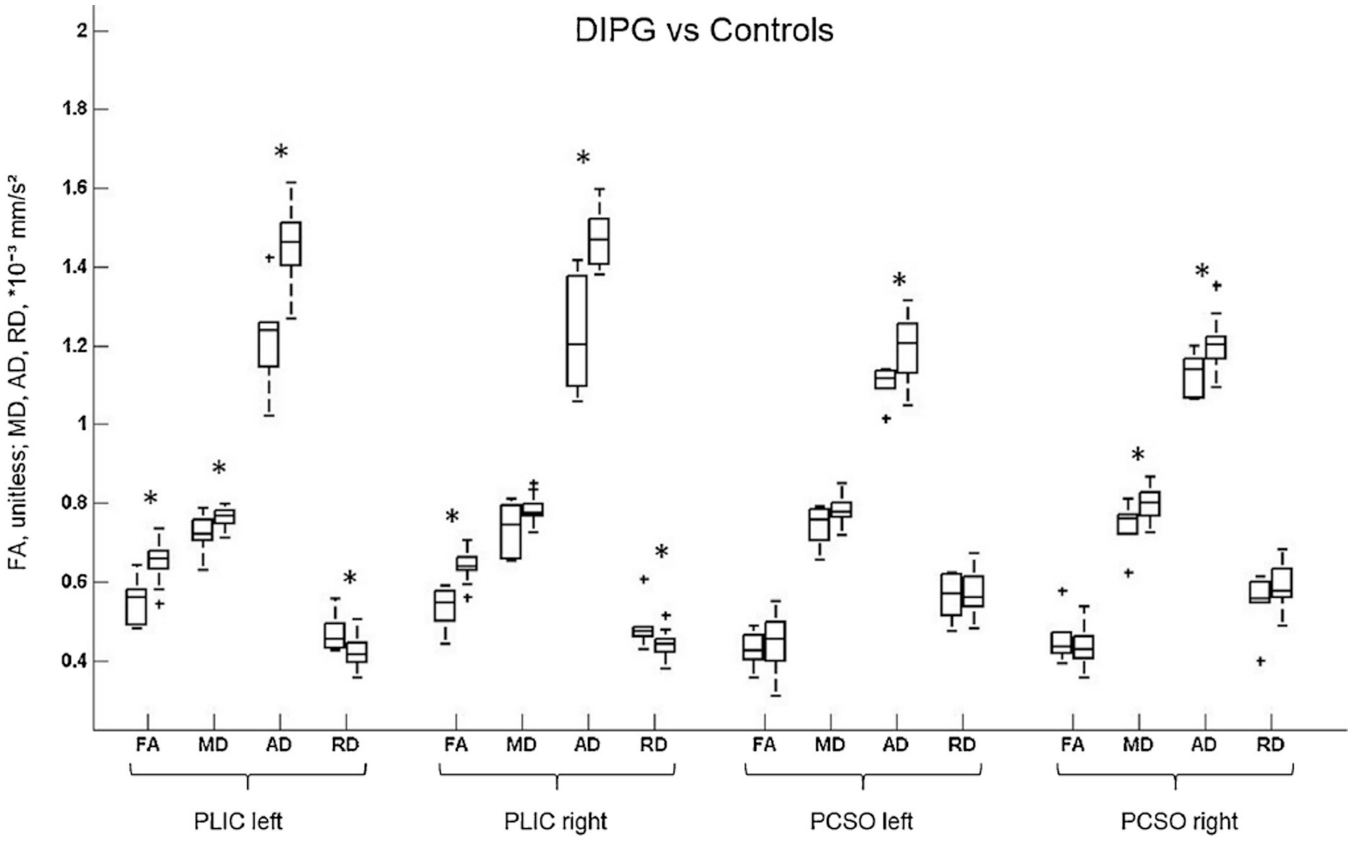

Fig. 2.

Box plots show changes in fractional anisotropy (FA) and mean (MD), axial (AD), and radial (RD) diffusivity at the level of the bilateral posterior limb of the internal capsule (PLIC) and bilateral posterior centrum semiovale (PCSO) in children with diffuse intrinsic pontine glioma (DIPG) compared to age-matched controls. * represents statistically significant differences. DIPGs are plotted first, controls second. Horizontal lines are median values, solid boxes show 25th to 75th centiles; whisker bars are 10th and 90th centiles; outliers are shown as pluses. * represents statistically significant differences.

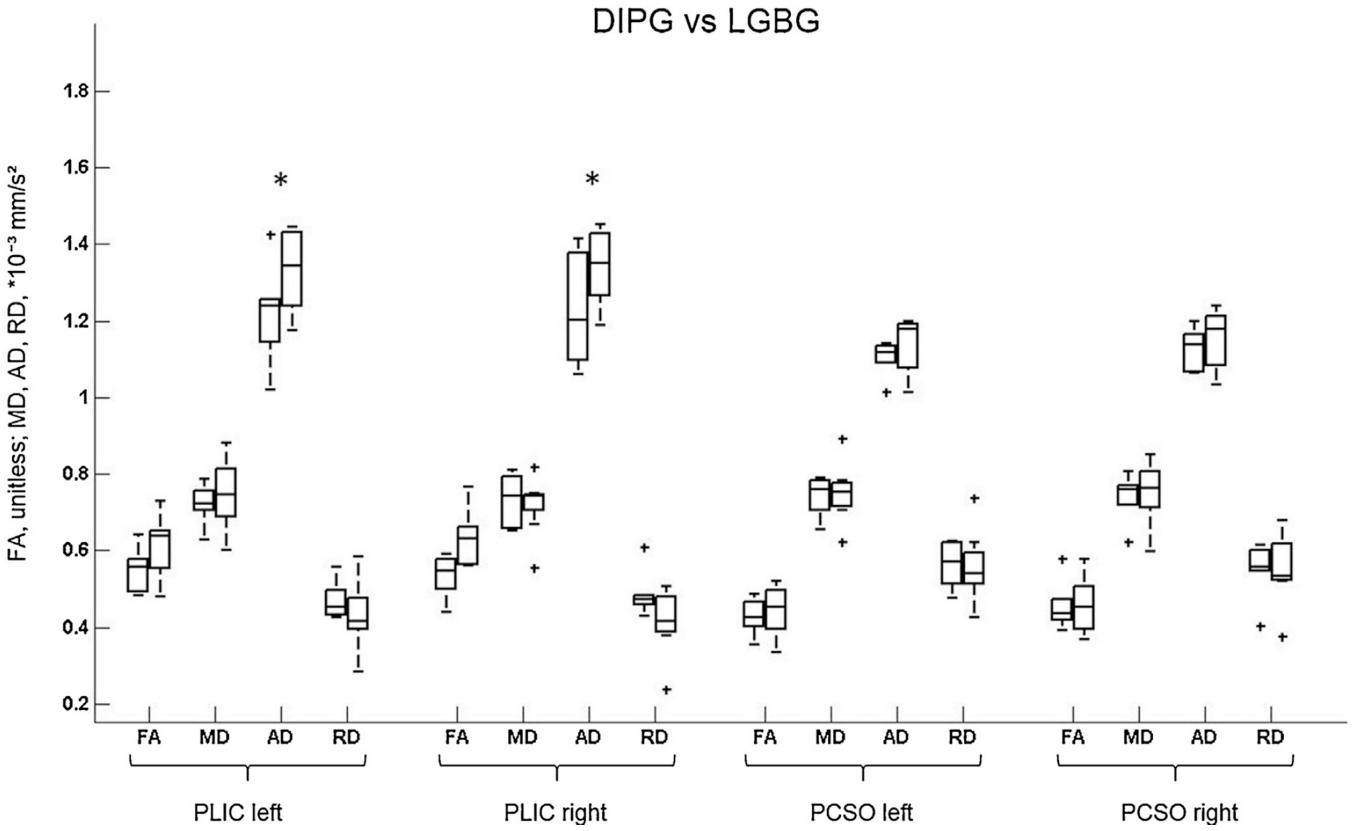

Fig. 3.

Box plots show changes in fractional anisotropy (FA) and mean (MD), axial (AD), and radial (RD) diffusivity at the level of the bilateral posterior limb of the internal capsule (PLIC) and bilateral posterior centrum semiovale (PCSO) in children with diffuse intrinsic pontine glioma (DIPG) and low-grade brain stem glioma (LGBG). DIPGs are plotted first, LGBGs second. Horizontal lines are median values, solid boxes show 25th to 75th centiles; whisker bars are 10th and 90th centiles; outliers are shown as pluses. * represents statistically significant differences.

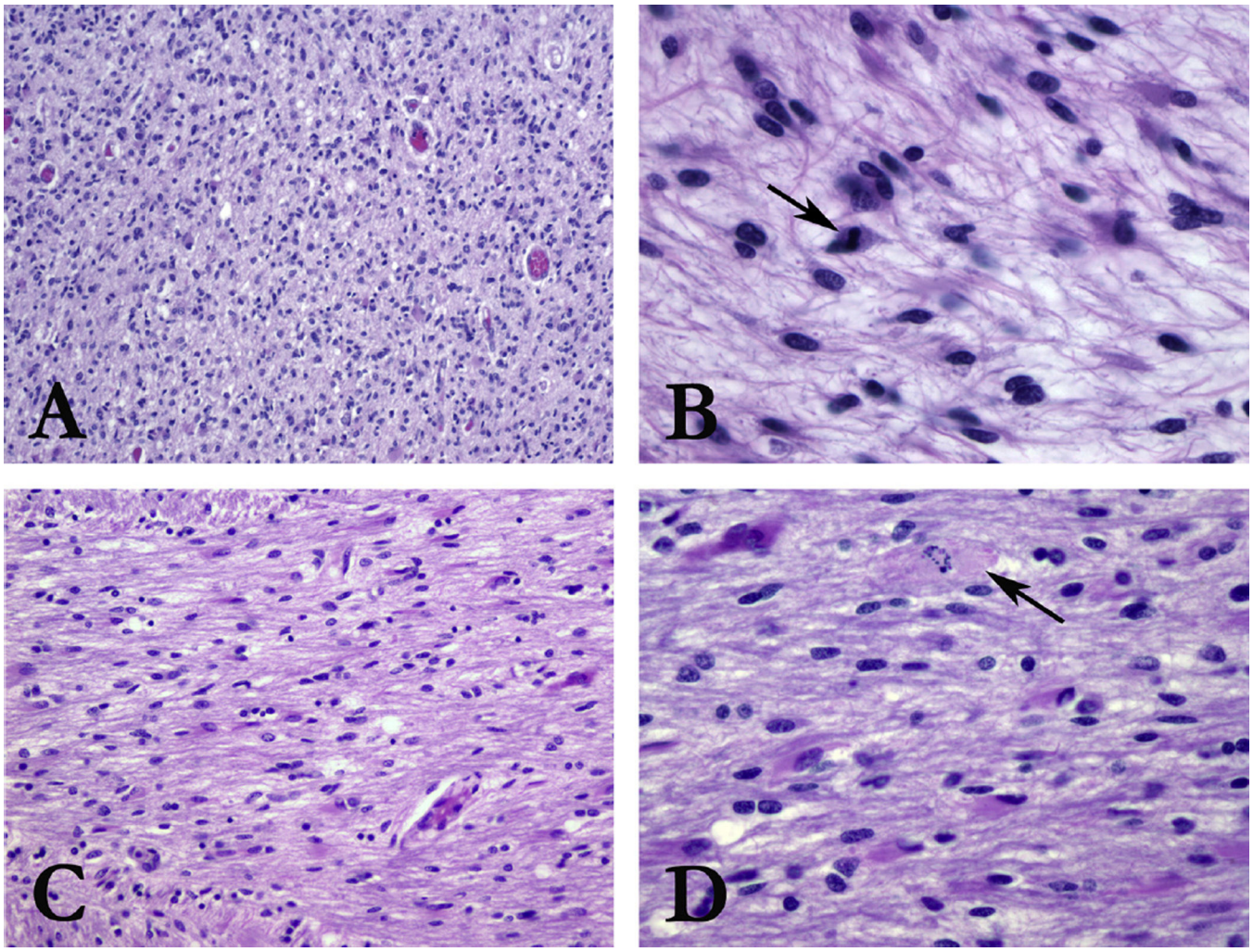

Fig. 4.

H&E histologic sections from the main tumor bulk in the pons show increased cellularity (A, 100×) with hyperchromatic, atypical astrocytic cells. Mitotic activity (arrow) is high (B, 400×), with areas of pseudopallisading necrosis (not shown), meeting criteria for glioblastoma (WHO Grade IV). Sections from the left PLIC show increased cellularity (C, 200×) with the same population of hyperchromatic, atypical astrocytic cells. Mitotic activity is elevated, including atypical forms (arrow) (200×) (D, 400×).

Table 1

Differences in DTI scalars between children with DIPG and age-matched controls.

		DIPG patients	Controls	*p*-value
		Mean ± SD	Mean ± SD	
PLIC	FA	0.552 ± 0.059	0.655 ± 0.043	**0.001**
left	MD (× 10^{-3} mm^2/s)	0.720 ± 0.054	0.763 ± 0.027	**0.048**
	AD (× 10^{-3} mm^2/s)	1.221 ± 0.133	1.453 ± 0.079	**0.001**
	RD (× 10^{-3} mm^2/s)	0.470 ± 0.051	0.418 ± 0.038	**0.02**
PLIC	FA	0.533 ± 0.056	0.643 ± 0.032	**<0.001**
right	MD (× 10^{-3} mm^2/s)	0.734 ± 0.070	0.780 ± 0.029	0.28
	AD (× 10^{-3} mm^2/s)	1.225 ± 0.145	1.468 ± 0.063	**<0.001**
	RD (× 10^{-3} mm^2/s)	0.488 ± 0.062	0.437 ± 0.033	**0.02**
PCSO	FA	0.427 ± 0.048	0.450 ± 0.063	0.33
left	MD (× 10^{-3} mm^2/s)	0.743 ± 0.053	0.782 ± 0.036	0.08
	AD (× 10^{-3} mm^2/s)	1.103 ± 0.047	1.198 ± 0.077	**0.02**
	RD (× 10^{-3} mm^2/s)	0.563 ± 0.059	0.574 ± 0.049	0.71
PCSO	FA	0.455 ± 0.066	0.438 ± 0.047	0.67
right	MD (× 10^{-3} mm^2/s)	0.741 ± 0.065	0.798 ± 0.038	**0.02**
	AD (× 10^{-3} mm^2/s)	1.129 ± 0.057	1.205 ± 0.062	**0.01**
	RD (× 10^{-3} mm^2/s)	0.547 ± 0.076	0.595 ± 0.047	0.13

AD, axial diffusivity; DIPG, diffuse intrinsic pontine glioma; FA, fractional anisotropy; MD, mean diffusivity; PCSO, posterior centrum semiovale; PLIC, posterior limb of internal capsule; RD, radial diffusivity; *p*-values from Wilcoxon rank sum tests, statistically significant differences are in bold.

Table 2

DTI scalars for children with DIPG and LGBG adjusted for age at MRI.

		DIPG Patients	LGBG Patients	
		LS Mean (95% CI)	**LS Mean (95% CI)**	***p*-value**
PLIC	FA	0.578 (0.514–0.641)	0.593 (0.539–0.647)	0.71
left	MD (× 10^{-3} mm^2/s)	0.688 (0.621–0.754)	0.771 (0.715–0.827)	0.08
	AD (× 10^{-3} mm^2/s)	1.190 (1.073–1.306)	1.354 (1.256–1.453)	**0.049**
	RD (×10^{-3} mm^2/s)	0.433 (0.377–0.490)	0.457 (0.409–0.504)	0.53
PLIC	FA	0.552 (0.492–0.613)	0.617 (0.566–0.668)	0.12
right	MD (× 10^{-3} mm^2/s)	0.703 (0.642–0.764)	0.744 (0.692–0.796)	0.32
	AD (× 10^{-3} mm^2/s)	1.188 (1.079–1.298)	1.369 (1.277–1.462)	**0.03**
	RD (× 10^{-3} mm^2/s)	0.460 (0.394–0.527)	0.434 (0.378–0.490)	0.55
PCSO	FA	0.443 (0.388–0.499)	0.432 (0.385–0.478)	0.74
left	MD (× 10^{-3} mm^2/s)	0.713 (0.660–0.767)	0.773 (0.728–0.818)	0.11
	AD (× 10^{-3} mm^2/s)	1.080 (1.024–1.136)	1.155 (0.107–1.202)	0.06
	RD (× 10^{-3} mm^2/s)	0.530 (0.464–0.596)	0.582 (0.527–0.638)	0.24
PCSO	FA	0.473 (0.406–0.539)	0.445 (0.388–0.501)	0.53
right	MD (× 10^{-3} mm^2/s)	0.711 (0.650–0.772)	0.773 (0.722–0.825)	0.14
	AD (× 10^{-3} mm^2/s)	1.103 (1.041–1.166)	1.172 (1.119–1.224)	0.11
	RD (× 10^{-3} mm^2/s)	0.515 (0.439–0.591)	0.574 (0.510–0.638)	0.25

AD, axial diffusivity; DIPG, diffuse intrinsic pontine glioma; FA, fractional anisotropy; LGBG, low-grade brain stem glioma; LS, least squares; MD, mean diffusivity; PCSO, posterior centrum semiovale; PLIC, posterior limb of internal capsule; RD, radial diffusivity; *p*-values from F tests, statistically significant differences are in bold.